

Axial Flux Synchronous Motors Test Stand

Abstract. The paper summarizes the design and development of the Axial Flux Synchronous Motors Test Stand constructed in the Łukasiewicz Research Network - Institute of Aviation in Warsaw. The test stand is fully automated and capable of measuring a wide variety of motor parameters thanks to high sampling rate of the data acquisition system and sophisticated LabView software tools. The safety of the entire installation is being monitored by an integrated safety system responsible for emergency shutdown of actuating devices when unsafe situation has been detected. The main goal of the presented test stand is to provide the efficiency map of the electrical machine being tested as a result of automatic two-dimensional speed-torque sweep with user defined resolution on both speed and torque axis.

Streszczenie. Artykuł ten podsumowuje projekt i budowę Hamowni Synchronicznych Silników Elektrycznych o Strumieniu Osiowym, która powstała w Instytucie Lotnictwa w Warszawie będącym częścią Sieci Badawczej Łukasiewicz. Opisywane stanowisko badawcze jest w pełni zautomatyzowane i ma możliwość mierzenia szerokiego zakresu parametrów silnika dzięki zastosowaniu systemu akwizycji danych o wysokiej prędkości próbkowania oraz dzięki opracowaniu zaawansowanych narzędzi programistycznych w środowisku LabView. Nad bezpieczeństwem całej instalacji czuwa zintegrowany ze stanowiskiem system bezpieczeństwa odpowiedzialny za zatrzymanie awaryjne urządzeń wykonawczych w przypadku wykrycia niebezpiecznej sytuacji. Głównym zadaniem prezentowanej hamowni jest opracowanie mapy sprawności badanego silnika jako rezultatu automatycznego przemiatania dwuwymiarowej przestrzeni prędkość-moment obrotowy o ustawianej przez użytkownika rozdzielczości osi prędkości i momentu obrotowego. (**Hamownia Synchronicznych Silników Elektrycznych o Strumieniu Osiowym**)

Keywords: axial flux, motor, test stand, power, measurement.

Słowa kluczowe: strumień osiowy, silnik, stanowisko badawcze, moc, pomiar.

Axial flux synchronous motors

Even though the aviation is one of the industries that has suffered the most due to the Covid-19 outbreak [1] it is forecasted that it will also be the one, that should recover the fastest, reaching the pre-pandemic number of passengers by the end of the year 2023 [2]. Once recovered the passenger number trend is estimated to behave in the same manner as it was observed previously, which means that more and more people will need to be transported by planes each following year. To accommodate this growing number of passengers the aviation carriers will need new, more efficient planes. One of the biggest costs of each airline is the jet fuel so even the slight improvement in the engines efficiency can amount to millions of dollars savings for the airlines [3]. When it comes to the turbofan jet engines there is a steady, however diminishing improvement in the fuel efficiency with each generation of new engines. If there is ever going to be a major leap in the plane propulsion fuel efficiency, we will need to switch from jet engines to electric motors. Beside the higher general efficiency of the electric motor over any type of fossil fuel combustion engine, the electric motor has the advantage of improving the aerodynamic efficiency of the plane by distributing the propulsion over the length of the wing by using high number of small electrically driven fans or propellers instead of two large turbofans [4]. Other advantages of electric propulsion include lower vibration and noise, less greenhouse gases emission, easier control and increased safety. The biggest factor hampering the development of aviation electrification is the energy density of energy storage. Even unmanned aerial vehicles using permanent magnet motors and a lithium polymer battery have a relatively low flight time. Therefore, a lot of research is conducted in order to develop technology enabling the increase in flight range using fuel cells [22].

If electric motors are ever going to be used for aircraft propulsion they will need to provide large rated power whilst complying with the constrains such as limited available space, required low weight and high efficiency [5]. Given these requirements the perfect candidate for aircraft propulsion are the permanent magnet machines, especially the axial flux permanent magnet motors due to their high

torque density, high compactness and high efficiency [5]. The electric motor test stand discussed in this paper has been designed with flexibility in mind so that virtually any type of motor could be tested using this test bench, however the initial focus was to test the axial flux permanent magnet motors first and the number one candidate has been the EMRAX 208 AC HV (Figure 1). This machine is a three phase synchronous, lightweight motor (power density up to 10kW/kg), that is highly efficient (92÷97%) and capable of producing high torque even at low speed [6]. The efficiency of the motor is given as a range due to its dependency on the drive cycle, thermal conditions and controller capability. Specific technical data of the chosen model:

- cooling – air,
- weight – 9.1kg,
- maximal rotation speed – 7000rpm,
- peak power – 75kW,
- continuous power - 20÷32kW,
- maximal battery voltage – 470Vdc,
- maximal current – 200Arms,
- continuous current – 100Arms,
- peak torque – 140Nm,
- continuous torque – 80Nm.

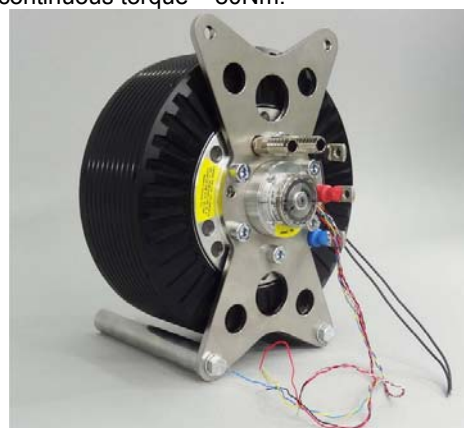


Figure 1 – EMRAX 208 axial flux permanent magnet motor (<https://emrax.com/e-motors/emrax-208/>)

Test stand block diagram

Figure 2 shows the block diagram of the electric motors test stand presented in this paper. At the heart of the system are two motors (of the same type) being tested. One of them acts as a motor (MOT-300) and the other one acts as a generator (GEN-370). The motors are coupled by a single shaft with torque meter installed in series (UT-340). All rotating devices within the test stand are enclosed in a cage (Figure 3) for safety purposes. Each of the motors is being controlled by its dedicated inverter (INV-200 and INV-400 respectively). The electrical parameters of the motors are measured by the devices installed in the BOX-200, BOX-201, BOX-400 and BOX-401 aluminum cabinets. In each of these boxes three measurements are taken: RMS line current (measured by Hall transducer), instantaneous line current (measured by the shunt resistor and immediately amplified from mV range to $-10\div 10\text{VDC}$) and instantaneous line-to-line voltage. Given the high electromagnetic noise of the cables carrying fast changing and high currents, such as the supply provided by the inverter [7] great attention has been given to proper shielding of both measurement and supply cables. The shields of the measurement cables has been grounded only on one end (at the data acquisition system side) and the inverters to motors power supply cables shields has been grounded on both sides. However, due to the presence of the current measuring shunt resistors in the circuit, the shields of the supply cables do not cover the entire length of the wires. Therefore, the shunt resistors has been installed inside aluminum cabinets to provide additional electromagnetic interference protection. The measurements of both the instantaneous power consumed by the motor and supplied by the generator is performed using two separate Aron circuits. In Aron circuit the instantaneous three phase power is calculated using only four measurement, two line currents and two line-to-line voltages [8]. The power measurement will be described using more detail in later chapters.

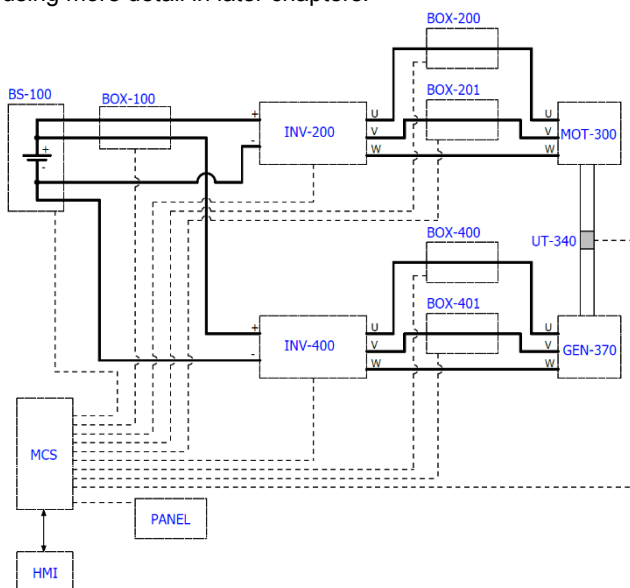


Figure 2 – electric motors test stand block diagram

The goal of the developed test stand is to conduct tests on motors that could be potentially used in aircraft propulsion systems. This kind of systems will use direct current as their power source, either from a battery pack or a fuel cell [9]. To mimic the conditions that the inverter and motor will encounter in their operation a battery simulator (BS-100 on Figure 2) has been used. A battery simulator is a device capable of simulating the output characteristics of

many pre-programmed batteries (such as lithium manganate, lithium cobalt oxide, lead-acid or lithium iron phosphate) or any custom battery by specifying its characteristic curve and parameters [10]. The battery simulator is capable of both supplying power to the motor's inverter and to simulate battery charging by receiving power from generator's inverter. The battery output voltage, output current and return current are all measured by devices installed in the BOX-100, therefore the battery output and return power can be easily calculated.



Figure 3 – rotating parts of the test stand enclosed in a cage

All the control, data acquisition and safety monitoring are performed by the Main Control System (MCS). The user can interact with the MCS in two manners:

- physical panel located in the control room – the control of the test stand using this panel can be performed only in manual mode; the panel displays current rotation speed of the motor and allows the user to control the speed of the motor and the torque of the generator using two separate knobs,
- human-machine interface – works in all modes of test stand operation; this is a LabView application that can be installed on any PC class computer; gives user full control of the test stand and visualizes the acquired data on charts (time and frequency) and on system's block diagram presented on the screen.

Power measurements

There is a total of five different power measurement taken at the test stand:

- the battery simulator output power $P_{\text{bat-out}}$ given by the equation **Błąd! Nie można odnaleźć źródła odwołania.**,
- the battery simulator return power $P_{\text{bat-ret}}$ given by the equation (2),
- the active power consumed by the motor P_{mot} given by equations (8) and (17),
- the active power produced by the generator P_{gen} given by equations (8) and (17),
- the mechanical power at the motor to generator coupling P_{mech} given by equation (19).

The battery simulator outputs a DC voltage and current which is then supplied to the DC bus of the inverter. Therefore, the power output of the battery simulator is a simple product of the DC voltage U_{bat} measured across the battery simulator output terminals and the DC current $I_{\text{bat-out}}$ measured in the positive lead connecting the battery and the motor's inverter:

$$(1) \quad P_{\text{bat-out}} = U_{\text{bat}} \cdot I_{\text{bat-out}}$$

Note: all the equations in this paper are given in a scalar form, unless explicitly stated otherwise.

On the side of the test stand the power returns from the generator's inverter DC bus to the battery simulator. Therefore, the power returned to the battery simulator is again a simple product of the DC voltage U_{bat} measured across the battery simulator output terminals and the DC current $I_{bat-ret}$ measured in the positive lead connecting the battery and the generator's inverter:

$$(2) \quad P_{bat-ret} = U_{bat} \cdot I_{bat-ret}$$

Measurement of the power consumed by the motor is a little more bit tricky. To accurately measure the instantaneous power of a three phase electrical machine it is required to measure three line currents and three line voltages. This is the so called three wattmeters method. In case of motors there is no neutral wire present in the circuit, therefore false neutral needs to be created by connecting the negative leads of the voltage measuring devices [11]. The three wattmeters method is advantageous when the power distribution over each phase is an important factor which is not the case when it comes to the test stand described (the only important parameter is the total power consumed/generated). In such case a two wattmeters or Aron connection method provides equally good results [11]. The advantage of the two wattmeters method is its simplified wiring and the fact that it can measure both balanced and unbalanced systems [12]. The other major advantage is that by measuring the two line currents and two line-to-line voltages the total power in the system can be calculated regardless of whether the load is connected in a star or delta configuration.

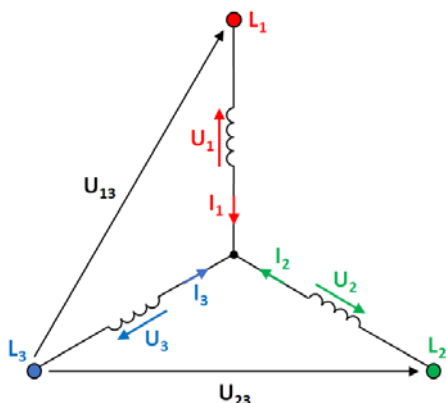


Figure 4 – two wattmeters method measuring power consumed by a load connected in a star configuration

Let's first consider the load in a star configuration (Figure 4). We are measuring two line currents (I_1 and I_2) and two line-to-line voltages (U_{13} and U_{23}) with respect to the phase in which the current is not measured (L_3). By using Kirchhoff's laws:

$$(3) \quad I_1 + I_2 + I_3 = 0 \rightarrow I_3 = -I_1 - I_2$$

$$(4) \quad U_{13} - U_1 + U_3 = 0 \rightarrow U_{13} = U_1 - U_3$$

$$(5) \quad U_{23} - U_2 + U_3 = 0 \rightarrow U_{23} = U_2 - U_3$$

Total apparent instantaneous power in the system can be calculated as:

$$(6) \quad P_{inst} = U_1 \cdot I_1 + U_2 \cdot I_2 + U_3 \cdot I_3$$

Substituting equation (3) into equation (6):

$$(7) \quad P_{inst} = U_1 \cdot I_1 + U_2 \cdot I_2 + U_3 \cdot (-I_1 - I_2) = U_1 \cdot I_1 + U_2 \cdot I_2 - U_3 \cdot I_1 - U_3 \cdot I_2 =$$

$$I_1 \cdot (U_1 - U_3) + I_2 \cdot (U_2 - U_3)$$

Substituting equation (4) and (5) into equation (7):

$$(8) \quad P_{inst} = U_{13} \cdot I_1 + U_{23} \cdot I_2$$

Equation (8) is the final calculation of the instantaneous power in a star connected load using the measured currents I_1 and I_2 and measured voltages U_{13} and U_{23} .

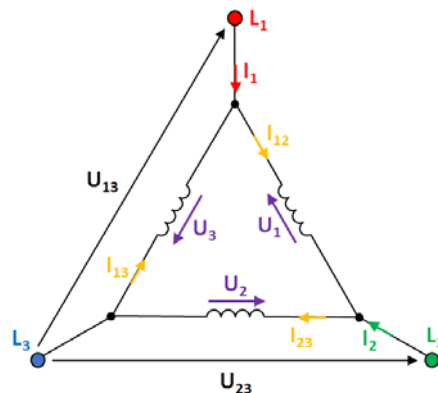


Figure 5 – two wattmeters method measuring power consumed by a load connected in a delta configuration

Now let's first consider the load in a delta configuration (Figure 5). Again, we are measuring two line currents (I_1 and I_2) and two line-to-line voltages (U_{13} and U_{23}) with respect to the phase in which the current is not measured (L_3). By using Kirchhoff's laws:

$$(9) \quad U_1 + U_2 + U_3 = 0 \rightarrow U_1 = -U_2 - U_3$$

$$(10) \quad I_1 + I_{13} - I_{12} = 0 \rightarrow I_1 = I_{12} - I_{13}$$

$$(11) \quad I_2 + I_{12} - I_{23} = 0 \rightarrow I_2 = I_{23} - I_{12}$$

Total instantaneous power in the system can be calculated as:

$$(12) \quad P_{inst} = U_1 \cdot I_{12} + U_2 \cdot I_{23} + U_3 \cdot I_{13}$$

Substituting equation (9) into equation (12):

$$(13) \quad P_{inst} = (-U_2 - U_3) \cdot I_{12} + U_2 \cdot I_{23} + U_3 \cdot I_{13} = -U_2 \cdot I_{12} - U_3 \cdot I_{12} + U_2 \cdot I_{23} + U_3 \cdot I_{13} = U_2 \cdot (I_{23} - I_{12}) + U_3 \cdot (I_{13} - I_{12})$$

Substituting equation (10) and (11) into equation (13):

$$(14) \quad P_{inst} = U_2 \cdot I_2 - U_3 \cdot I_1$$

Finally by observing that voltage U_{23} is equal to U_2 and that voltage U_{13} is equal and opposite to U_3 (the voltage drop in the wires connecting the machine to the source is negligible) we get the equation (15):

$$(15) \quad P_{inst} = U_{13} \cdot I_1 + U_{23} \cdot I_2$$

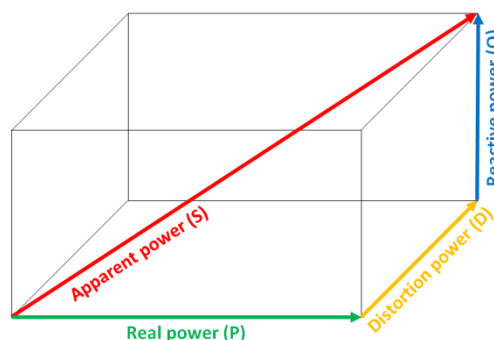


Figure 6 – three dimensional power triangle

Equation (15) is the final calculation of the instantaneous power in a delta connected load using the measured currents I_1 and I_2 and measured voltages U_{13} and U_{23} . It can be observed that equation (15) is exactly the same as equation (8), which proves that by using the Aron connection the total instantaneous power can be measured in both star and delta connected loads with no required changes.

When there is an inverter present in the circuit the load becomes highly non-linear and the power vectors relationship has to be taken into account. When the load is non-linear this relationship differs from the well-known power triangle and becomes three dimensional (Figure 6) to account for the distortion power caused by the harmonics [13]. The distortion power does not contribute to any useful work just like the apparent power. There are two power factors to consider – the displacement power factor and distortion power factor. The displacement power factor is the angle difference between the fundamental components of voltage and current signals (just like in the two dimensional power triangle). The distortion power factor is affected by the total harmonic content of the system. The apparent power can be calculated using equation (16):

$$(16) \quad S = \sqrt{P^2 + Q^2 + D^2}$$

It is important to keep this relationship in mind, however when the instantaneous power in the system is calculated the active power consumed by the load can be obtained [14] by simple integration over time T – equation (17). Preferably the integration time should be a product of the period τ of the fundamental voltage component and any integer number – equation (18). Increasing the integer number k value leads to greater accuracy of the real power measurement but decreases the response time.

$$(17) \quad P = \frac{1}{T} \cdot \int_t^{t+T} P_{inst}(t) dt$$

$$(18) \quad T = k \cdot \tau, \quad k = 1, 2, 3, \dots$$

Last unknown power in the system is the mechanical power P_{mech} , that can be easily calculated [15] using signals measured by the torque meter – equation (19). Any modern torque meter has three outputs – the torque measurement itself and two pulse signals [16]. The pulse signals can be used to accurately calculate the rotation speed and to establish the rotation direction. The torque meter used at the presented test stand has two pulse outputs, giving 360 pulses per revolution. The pulses at each output are displaced by 90° with respect to each other to provide the information needed to establish the direction of rotation. By calculating the time elapsed between the rising edges of the pulse signal, the rotation speed can be obtained. The pulse signal is produced by sensors detecting the presence of a tooth in a wheel. To produce 360 pulses, there has to be 360 teeth in the wheel. Due to the machining imperfections the best accuracy of speed measurement is obtained when the time elapsed is measured for the duration of one full rotation. In that scenario the clock is started when the first rising edge occurs. At this moment the internal counter is set to zero. Then the internal counter is incremented by one any time a rising edge is detected. When the internal counter reaches 360, the current clock time t_{360} is stored, the clock is restarted, and the internal counter set back to zero. Then the whole cycle repeats. By using this approach any error caused by teeth machining imperfections is neglected due to the fact that the time used for speed calculation is the time elapsed between rising edges of the pulse signal triggered by the exact same tooth. The only drawback of this method is that the speed is updated only

once every revolution. This issue has been addressed by implementing two separate speed measurements: one accurate (360 pulses considered for calculation) and one coarse (10 pulses considered for calculation). The rotation speed is calculated using the equation (20).

$$(19) \quad P_{mech} = T \cdot \omega = T \frac{2 \cdot \pi \cdot n_{rpm}}{60}$$

$$(20) \quad n_{rpm} = \frac{60}{t_{360}}$$

Efficiencies

Due to the several power measurements taken at the test stand, it is possible to calculate a wide variety of system efficiencies:

- motor efficiency η_{mot} given as the ratio of the mechanical power measured at the shaft and the power consumed by the motor – equation (21),
- generator efficiency η_{gen} given as the ratio of the power generated by the generator and the mechanical power measured at the shaft – equation (22),
- inverter efficiency when working as a load $\eta_{inv-mot}$ given as the ratio of power consumed by the motor and the power supplied by the battery simulator – equation (23),
- inverter efficiency when working as a supply $\eta_{inv-gen}$ given as the ratio of power returned to the battery simulator and the power generated by the – equation (24),
- total system efficiency η_{tot} given as the ratio of power returned to the battery simulator and the power supplied by the batter simulator – equation (25).

$$(21) \quad \eta_{mot} = \frac{P_{mech}}{P_{mot}} \cdot 100\%$$

$$(22) \quad \eta_{gen} = \frac{P_{gen}}{P_{mech}} \cdot 100\%$$

$$(23) \quad \eta_{inv-mot} = \frac{P_{mot}}{P_{bat-out}} \cdot 100\%$$

$$(24) \quad \eta_{inv-gen} = \frac{P_{bat-ret}}{P_{gen}} \cdot 100\%$$

$$(25) \quad \eta_{tot} = \frac{P_{bat-ret}}{P_{bat-out}} \cdot 100\%$$

[Nm] Torque					
70	93,74	93,66	94,31	95,61	>92
60	93,15	93,03	93,49	94,52	>93
50	92,77	92,68	93,02	93,82	>94
40	92,83	92,70	92,86	93,34	>95
30	93,17	93,13	93,11	93,19	
20	93,75	93,77	93,59	93,23	
10	94,46	94,62	94,26	93,43	Speed
	500	1000	1500	2000	[rpm]

Figure 7 – example of the efficiency map prepared by the system

All the aforementioned efficiencies are measured and displayed by the system, however the two efficiencies of the highest interest are the motor efficiency and the generator efficiency. Only these two parameters are used to prepare the efficiency maps the are the main goal of conducting the tests using the presented electrical motors test stand. Figure 7 shows an example of the motor efficiency map prepared by the system using the measurements acquired during a two-dimensional speed-torque sweep. The coloring of the map adjusts automatically to the presented range of efficiencies.

Main control system

Main Control System (MCS) refers to all the hardware and software that supplies the power to the motors, controls the actuating devices, monitors all sub-systems and acquires all the data. At the heart of the MCS is a National Instruments cRIO-9038 controller equipped with 8 communication, inputs, outputs and safety cards. A great deal of effort was put into designing, coding and testing the software dedicated for this electric motor test stand. Figure 8 shows the architecture of this software which consist of four separate main parts: FPGA (field programmable gate array) application, real-time operating system application, HMI (human-machine interface) application (running on Windows) and safety application. The analysis of Figure 8 reveals that the FPGA and safety applications are separate pieces of software, however they are both managed by the real-time target (RT target) application. The HMI and RT target are communicating with each other using the network stream, which is a point-to-point communication type that maintains the data until it is transferred or until the connection fails [17]. Due to the criticality of data being transferred between HMI and RT target (control messages, safety monitoring data, etc.) this feature of the network stream makes it a perfect tool for the communication purposes.

All the critical system operations, such as control, data acquisition and test parameters calculation, are being performed by the FPGA and real-time operating system. FPGA application runs all the intensive and critical tasks, therefore freeing the processor time for other operations. This configuration enables an extremely high throughput and a deterministic execution of operations. FPGA is programmed in a manner similar to any other LabView application, but it is important to remember that it is a hardware application and therefore it is directly connected to all the physical outputs and inputs. Such architecture provides an unparalleled performance of operations like synchronization, triggering, customizable timing and signal processing [18].

RT target application runs on top of the FPGA and is used to calculate the critical system parameters and acquire, process and store large amounts of data. The application is managed by a real-time operating system (NI

Linux Real-Time developed by National Instruments) which is fully deterministic. The determinism of the software means that important tasks chosen by the application developer will always execute in the pre-determined amount of time [19]. NI Linux Real-Time ensures such deterministic execution of critical operations. Furthermore, it is highly robust (recovery without any noticeable disruption in case of failure), facilitates multitasking for parallel execution of several tasks at once and provides a proven and stable network stack [20].

The HMI application allows user to operate electrical motors test stand and to communicate with motor and generator inverters and the battery simulator. The application can be displayed on two screens. First screen is used to visualizes the system current state and allows the user to control the test stand (Figure 9). Second screen can be used either for displaying the current data on graphs (time domain or frequency domain) or for displaying the efficiency map prepared for the data acquired during the test currently in progress. The major tasks performed by the HMI application are the following:

- set motor and generator parameters (speed, torque, number of poles, etc.)
- set battery simulator parameters (battery type, state of charge, internal resistance, voltage, current, etc.),
- display real-time data on charts,
- display the FFT data on charts,
- display the efficiency maps,
- display the system state data using the monitoring icons,
- display current system measurements and parameters on the visualization,
- program automated two-dimensional speed-torque sweeps,
- configure channels' scaling and filtering,
- configure alarms,
- create new channels by combining other channels and using basic mathematical operators,
- add users and set users permissions,
- enable/disable controls based on the permission set of the user currently logged in.

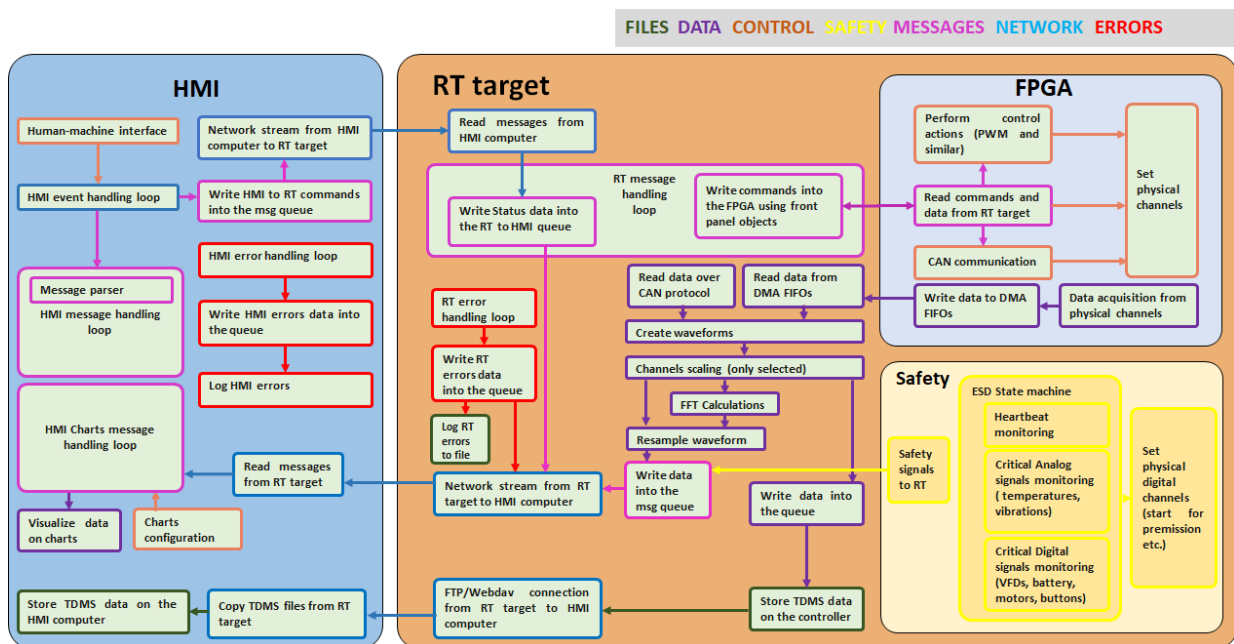


Figure 8 – main control system software architecture

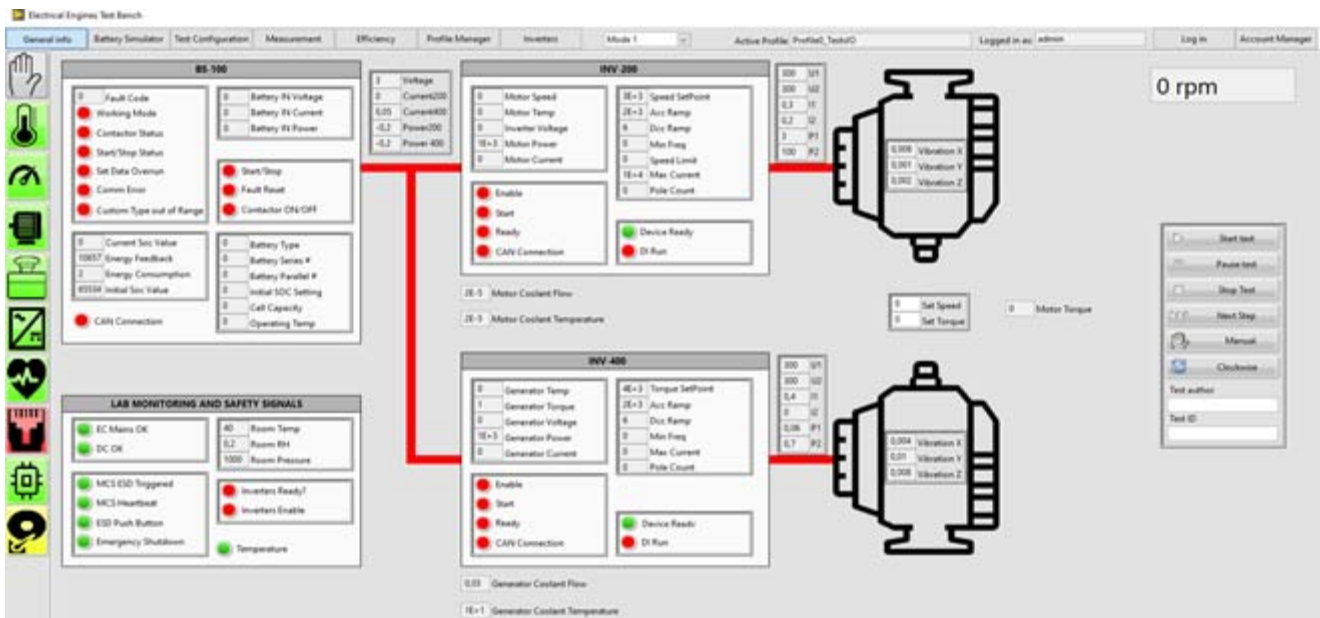


Figure 9 – the main screen of the human-machine interface application

Safety system

Safety system monitors all the critical system parameters and can trigger an emergency shutdown procedure which stops and blocks all the actuating devices. The safety application is managed and run by National Instruments SIL3 capable safety card NI-9350, which uses algorithms implemented with software state machines to run self-contained logic operations [21]. This card uses one of the slots in the NI compactRIO master controller, however it is powered by a separate cable. The connection with the controller serves only for reading the inputs, outputs, and internal states of the safety card, that can be then displayed to the user using the HMI application. The implemented safety logic will cause the emergency shutdown procedure in the following cases:

- either of the emergency shutdown buttons has been pressed (there are two such buttons – one installed on the front door of the MCS cabinet and second on the operator's panel in the control room),
- the 24Vdc power supply in the MCS cabinet has failed,
- the battery simulator power supply has failed,
- the temperature in the test cell has reached a predefined threshold,
- the heart-beat signal generated by the master controller is corrupted (master controller generates a heart-beat signal in a form of 1Hz square wave; the safety system monitors this signal by measuring the time elapsed between its subsequent raising/falling edges; the heart-beat is considered to be corrupted in the case when the measured elapsed time is outside of 450÷550ms range),
- the master controller requests the emergency shutdown procedure due to user defined alarm being activated (the user can configure an alarm value on any channel, for example motor vibration, motor internal temperature or torque; if later during system's operation this alarm value is exceeded, the master controller will request the emergency shutdown procedure to be activated).

Regardless of the cause, the emergency shutdown procedure it is always realized by deactivating the coils of

two redundant relays that supply the enable signal to all the actuating devices. Once the enable signal is deactivated, the actuating devices are stopped and prevented from running until the enable signal is activated again. Once all the signals monitored by the safety system are back to their safe state the emergency shutdown procedure can be cleared by pressing the reset button on the operator's panel in the control room. Only then the actuating devices are permitted to start operating again.

Summary

The electrical motors test stand presented in this paper is a fully automated, modern test bench capable of acquiring the efficiency map of any small and mid-size electrical motor. The implemented software enables to control and monitor all the actuating devices in a broad and unrestricted range, whilst not worrying about exceeding any operating safety limits thanks to the safety system monitoring all the important parameters. All the important test measurements are presented to the user in a clear and informative form what makes the testing even more effective.

Authors:

Łukasz Kędzierski, Faculty of Electrical Engineering, Warsaw University of Technology, Pl. Politechniki 1, 00-661 Warsaw, E-mail: lukasz.kedzierski.dokt@pw.edu.pl

Rafał Sikorski, Faculty of Electrical Engineering, Warsaw University of Technology, Pl. Politechniki 1, 00-661 Warsaw, E-mail: rafal.sikorski.dokt@pw.edu.pl

Przemysław Wyszowski, Łukasiewicz Research Network – Institute of Aviation, Aleja Krakowska 110/114, 02-256 Warsaw, E-mail: przemyslaw.wyszowski@ilot.lukasiewicz.gov.pl

Mateusz Bartela, Łukasiewicz Research Network – Institute of Aviation, Aleja Krakowska 110/114, 02-256 Warsaw, E-mail: mateusz.bartela@ilot.lukasiewicz.gov.pl

REFERENCES

- [1] David Melas, Katarina Melasova, "The Early Impact of Covid-19 Pandemic on the Aviation Industry", Acta Avionica, Volume XXII, 42 – No.1, 2020
- [2] Sveinn Vidar Gudmundsson, Renato Redondi, Mattia Cattaneo, "Forecasting recovery time in air transport markets in the presence of large economic shocks: COVID-19", Reykjavik University, November 28, 2020

- [3] Mark Camilleri, "Aircraft Operating Costs and Profitability", *Travel Marketing, Tourism Economics and the Airline Product*, Chapter 12, pp. 191-204
- [4] David Deisenroth, Michael Ohadi, "Thermal Management of High-Power Density Electric Motors for Electrification of Aviation and Beyond", *Energies* 2019, 12, 3594
- [5] Zhuoran Zhang, et al., "Feasibility of a New Ironless-stator Axial Flux Permanent Magnet Machine for Aircraft Electric Propulsion Application", *CES Transactions on Electrical Machines and Systems*, Vol. 3, No. 1, March 2019
- [6] "User's Manual for Advanced Axial Flux Synchronous Motors and Generators", EMRAX, August 2018
- [7] Mathieu Sarrazin, Karl Janssens, Herman Van der Auweraer, "Influence of inverter PWM control schemes on noise signature of electric powertrains", 20th International Congress on Sound & Vibration, Bangkok, 7-11 July 2013
- [8] T. Rudnicki, A. Sikora, R. Czerwiński, D. Polok, "Impact of PWM Control Frequency onto Efficiency of a 1 kW Permanent Magnet Synchronous Motor (PMSM)", *Elektronika ir Elektrotechnika*, Vol. 22, No. 6, 2016, pp. 10-16
- [9] Jeffrey Collins, Dustin McLarty, "All-electric commercial aviation with solid oxide fuel cell-gas turbine battery hybrids", *Applied Energy* 265, 2020
- [10] "DC Power Supply Series - User Manual", Kewell Power System Co., Version Number K-DCPSC-201804, 2018
- [11] "The Fundamentals of Three-Phase Power Measurements", Application Note, Tektronix, 2013
- [12] "Fundamentals of Electric Power Measurements", Yokogawa, May 2020
- [13] Shantanu Das, "Note on Harmonic Distortion Control & Power Factor Correction Circuitry for Switched Mode Power Supply (M+N)", *Reactor Control Systems Design Section E&I Group B.A.R.C.*, December 2016
- [14] S. V. Myatezh, et al., "Definition of distortion power in AC network and analysis of its reasons", *IOP Conference Series: Materials Science and Engineering*, 2019
- [15] Marcin Baszyński, Stanisław Piróg, "Determining the mechanical losses in a high-speed motor on the example of a flywheel energy storage system", *Archives of Electrical Engineering*, 2012, Vol. 61, pp. 299-313
- [16] "Rotating Torque Sensors: DR-2212/DR-2212-P", Lorenz Messtechnik GmbH, 2020
- [17] Barlian Henryranu Prasetio, Dahnial Syauqy, Rizal Maulana, Gembong Edhi Setyawan, "Study of voice data communication using network streams on dataflow programming", *MATEC Web of Conferences* 154, 2018
- [18] "The LabVIEW RIO Architecture: A Foundation for Innovation", National Instruments, 2020
- [19] A. Viana, O.R. Polo, P. Parra, "Increasing the Determinism in Real-Time Operating Systems for ERC32 Architecture", *Proceedings of the 5th WSEAS Int. Conf. on Software Engineering, Parallel and Distributed Systems*, Madrid, Spain, February 15-17, 2006, pp 110-116
- [20] "Introduction to NI Linux Real-Time", National Instruments, 2020
- [21] "NI 9350 Datasheet", National Instruments, November, 2017
- [22] Jan M. Krawczyk, et al., "Fuel Cells as Alternative Power for Unmanned Aircraft Systems – Current Situation and Development Trends", *Transactions of the Institute of Aviation*, no. 237, Warsaw 2014